Proceedings of the Eighteenth International Conference on
Civil, Structural and Environmental Engineering Computing
Edited by: P. Iványi, J. Kruis and B.H.V. Topping
Civil-Comp Conferences, Volume 10, Paper 6.2
Civil-Comp Press, Edinburgh, United Kingdom, 2025
ISSN: 2753-3239, doi: 10.4203/ccc.10.6.2

Influence of Soil Particle Distribution on the Steady-State Harmonic Response of Nonlinear Soil-Structure Interaction Systems

F. Maksimov[1], A. Contento[2], B. Briseghella[2] and P. Cacciola[2]

[1]School of Architecture, Technology and Engineering, University of Brighton, UK
[2]College of Civil Engineering, Fuzhou University, China

Abstract

This study investigates the steady-state harmonic response of nonlinear soil–structure interaction (SSI) systems. A lumped parameter model is adopted, in which the soil is represented by nonlinear springs and dashpots to capture its dynamic behaviour. Using the harmonic balance method, amplitude-dependent equivalent stiffness and damping parameters are derived to characterise the nonlinear SSI response. A Monte Carlo framework is employed to determine these amplitude-dependent properties across multiple soil configurations generated via the Discrete Element Method (DEM), accounting for the variability in particle distribution. The influence of this variability on the dynamic response of structures is examined through statistical analyses of the equivalent fundamental period and damping, both as functions of excitation amplitude. The methodology is demonstrated for two soil types: conventional gravel and a more innovative rubber–soil mixture.

Keywords: nonlinear soil-structure interaction, distinct element method, soil uncertainty, soil particle distribution, harmonic balance, steady state response.

1 Introduction

Soil–structure interaction (SSI) studies can be traced back to the late 19th century [1]. The analysis of the response of an infinite (or semi-infinite) elastic medium represented the initial approach, which remains in use by researchers and practitioners today [2], [3]. However, due to the inherent nonlinear behaviour of the soil medium, the nonlinear SSI problem has been extensively investigated over the

past five decades, as the assumption of linear SSI is not always appropriate or beneficial [4], [5]. Despite the high accuracy achievable through finite element (FE) models, simplified models continue to play a significant role in SSI studies. These models, while requiring reduced computational effort, enable comprehensive parametric analyses and offer valuable insights into the influence of key physical parameters [6]. Recent contributions [7–13] have investigated simplified nonlinear spring models designed to capture essential characteristics of nonlinear SSI, such as changes in equivalent period and foundation damping. The influence of modelling simplifications on the uncertainty of seismic response in numerical simulations that include SSI has been examined through a real case study in [14], while a broader overview of the various types of uncertainties inherent in SSI is provided in [15].

In this study, the influence of soil particle distribution on dynamic SSI is investigated. The Discrete Element Method (DEM) is employed within a stochastic framework to simulate multiple SSI models, wherein the soil is characterised by a prescribed granulometric distribution. This results in spatially randomised, non-overlapping particle configurations that reflect the inherent uncertainties of real soil materials. A Monte Carlo analysis is conducted over numerous realizations of these configurations to quantify the impact of variability in particle size distribution and packing structure on the lateral and rotational stiffness and damping of shallow foundations.

Furthermore, for each realization, the steady-state response of a simplified nonlinear SSI system is analysed. To this end, the harmonic balance method [16], [17], as extended in [12] to nonlinear SSI problems, is applied. The steady-state solution is obtained by solving, for each realisation, a set of nonlinear algebraic equations. In addition, the variability of the equivalent fundamental SSI period induced by differences in soil particle distribution is also assessed.

2 Methods

Consider the multi-degree-of-freedom (m-DoF) system illustrated in Figure 1a. The superstructure is assumed to behave linearly, while the foundation is considered rigid and supported by a nonlinear, compliant soil medium. The SSI mechanism is represented by two uncoupled nonlinear hysteretic springs, as shown in Figure 1b. The equation of motion of the system subjected to a dynamic load vector $\boldsymbol{p}(t)$ is given by:

$$\boldsymbol{M}\ddot{\boldsymbol{u}}(t) + \boldsymbol{C}\dot{\boldsymbol{u}}(t) + \boldsymbol{K}\boldsymbol{u}(t) + \boldsymbol{h}(t) = \boldsymbol{p}(t) \tag{1}$$

where $\boldsymbol{u}(t)$ is the displacement vector, $\boldsymbol{M}$, $\boldsymbol{C}$, and $\boldsymbol{K}$ are the mass, damping, and stiffness matrixes, respectively. Additionally, $\boldsymbol{h}(t)$ is the nonlinear hysteretic vector encompassing the nonlinear forces generated by the soil springs, i.e., the horizontal force f_h and the moment f_θ (see Figure 1b and 1c).

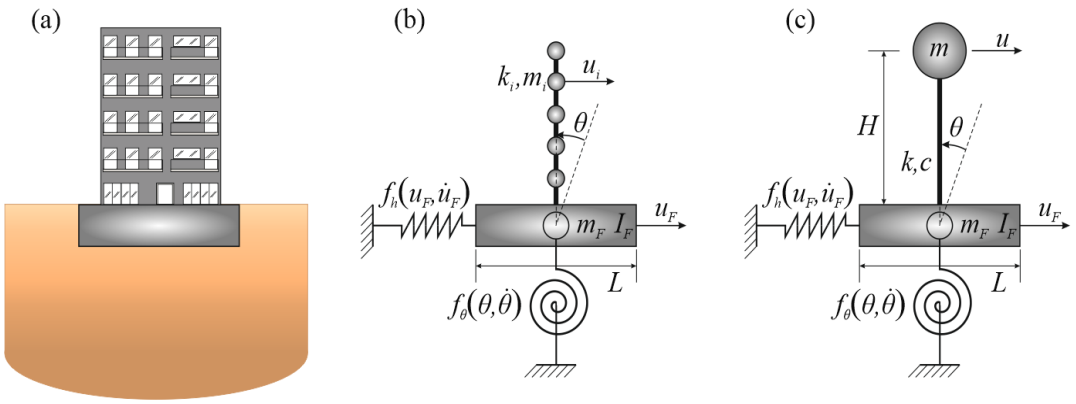

Figure 1: Structure resting over a non-linear compliant soil (a) and its discretization (b); 3-DoF lumped mass model (c).

For the simplest case (Figure 1c) of 3-DoF nonlinear soil-structure coupled system ($i.e.\ \boldsymbol{u}(t) = [u\ u_F\ \theta]^T$) those matrixes reduce to

$$\boldsymbol{M} = \begin{bmatrix} m & 0 & 0 \\ 0 & m_F & 0 \\ 0 & 0 & I_F \end{bmatrix} \tag{2}$$

where m is the superstructure mass, m_F is the foundation mass, I_F is the foundation moment of inertia;

$$\boldsymbol{K} = \begin{bmatrix} k & -k & -k\,H \\ -k & k & k\,H \\ -k\,H & k\,H & k\,H^2 \end{bmatrix} \tag{3}$$

in which k is the superstructure lateral stiffness and H the height of the superstructure;

$$\boldsymbol{C} = \begin{bmatrix} c & -c & 0 \\ -c & c & 0 \\ 0 & 0 & 0 \end{bmatrix} \tag{4}$$

with c being the viscous damping of the superstructure. Additionally, the hysteretic term can be written as

$$\boldsymbol{h}(t) = [0 \quad f_h(u_F, \dot{u}_F) \quad f_\theta(\theta, \dot{\theta})]^T \tag{5}$$

where $f_h(u_F, \dot{u}_F)$ and $f_\theta(\theta, \dot{\theta})$ are the nonlinear hysteretic elements pertinent to the translational and rotational foundation degrees of freedom u_F and θ, respectively.

In order to determine the steady-state harmonic response of the soil-structure systems governed by Eq. (1) the loading term is assumed to be a harmonic excitation, i.e., $\boldsymbol{p}(t) = \boldsymbol{p}_0\, cos(\,\omega t)$, with $\boldsymbol{p}_0$ the vector listing the input amplitudes, ω the circular frequency and t is the time. Following the harmonic balance approach [16] and [17] the response is assumed to exhibit a pseudo-harmonic behavior, that is

$$u_F(t) = a_h(t)\, cos(\,\omega t + \phi(t)), \qquad \dot{u}_F(t) = -a_h(t)\omega\, sin(\,\omega t + \phi(t)), \tag{6}$$

and

$$\theta(t) = a_\theta(t)\, cos(\,\omega t + \phi(t)), \quad \dot{\theta}(t) = -a_\theta(t)\omega\, sin(\,\omega t + \phi(t)), \tag{7}$$

in which the amplitudes $a_h(t)$ and $a_\theta(t)$ and the phase $\phi(t)$ are assumed slowly varying with respect to time. The nonlinear terms $f_h(u_F, \dot{u}_F)$ and $f_\theta(\theta, \dot{\theta})$ are, therefore replaced, in a harmonic balance sense, by the expressions ([17], [18])

$$f_h(u_F, \dot{u}_F) = c_{e,h}(a_h)\dot{u}_F + k_{e,h}(a_h)u_F, \tag{8}$$

where

$$c_{e,h}(a_h) = -\frac{1}{\pi\omega a_h}\int_0^{2\pi} f_h(a_h\, cos\,\vartheta\,, -a_h\omega\, sin\,\vartheta)\, sin\,\vartheta\, d\vartheta, \tag{9}$$

and

$$k_{e,h}(a_h) = \frac{1}{\pi a_h}\int_0^{2\pi} f_h(a_h\, cos\,\vartheta\,, -a_h\omega\, sin\,\vartheta)\, cos\,\vartheta\, d\vartheta\,, \tag{10}$$

are the equivalent horizontal damping and stiffness, respectively. Similarly,

$$f_\theta(\theta, \dot{\theta}) = c_{e,\theta}(a_\theta)\dot{\theta} + k_{e,\theta}(a_\theta)\theta, \tag{11}$$

where

$$c_{e,\theta}(a_\theta) = -\frac{1}{\pi\omega a_\theta}\int_0^{2\pi} f_\theta(a_\theta\, cos\,\vartheta\,, -a_\theta\omega\, sin\,\vartheta)\, sin\,\vartheta\, d\vartheta, \tag{12}$$

and

$$k_{e,\theta}(a_\theta) = \frac{1}{\pi a_\theta}\int_0^{2\pi} f_\theta(a_\theta\, cos\,\vartheta\,, -a_\theta\omega\, sin\,\vartheta)\, cos\,\vartheta\, d\vartheta\,, \tag{13}$$

are the equivalent rotational damping and stiffness. The equivalent linear system of Eq. (1) is, therefore, rewritten as:

$$\boldsymbol{M}\ddot{\boldsymbol{u}}(t) + (\boldsymbol{C} + \boldsymbol{C}_e(a_h, a_\theta))\dot{\boldsymbol{u}}(t) + (\boldsymbol{K} + \boldsymbol{K}_e(a_h, a_\theta))\boldsymbol{u}(t) = \boldsymbol{p}_0\, cos(\,\omega t) \tag{14}$$

where $\boldsymbol{K}_e(a_h, a_\theta)$ and $\boldsymbol{C}_e(a_h, a_\theta)$ are the equivalent stiffness and equivalent damping matrixes, respectively. To be more specific, in the case of the 3-DoF system shown in Figure 1c, $\boldsymbol{K}_e(a_h, a_\theta)$ and $\boldsymbol{C}_e(a_h, a_\theta)$ assume the following form:

$$\boldsymbol{K}_e(a_h, a_\theta) = \begin{bmatrix} 0 & 0 & 0 \\ 0 & k_{e,h}(a_h) & 0 \\ 0 & 0 & k_{e,\theta}(a_\theta) \end{bmatrix}, \tag{15}$$

and

$$\boldsymbol{C}_e(a_h, a_\theta) = \begin{bmatrix} 0 & 0 & 0 \\ 0 & c_{e,h}(a_h) & 0 \\ 0 & 0 & c_{e,\theta}(a_\theta) \end{bmatrix}. \quad (16)$$

The steady-state response is finally determined by the equation

$$\boldsymbol{U}(a_h, a_\theta; \omega) = [(\boldsymbol{K} + \boldsymbol{K}_e(a_h, a_\theta)) + i\omega(\boldsymbol{C} + \boldsymbol{C}_e(a_h, a_\theta)) - \omega^2 \boldsymbol{M}]^{-1} \boldsymbol{p}_0, \quad (17)$$

which represents a nonlinear algebraic equation whose solution can be pursued by traditional numerical techniques.

The analysis of Equations (15)-(17) highlights that a key challenge lies in the accurate evaluation of the amplitude-dependent stiffness and damping parameters, namely $k_{e,h}(a_h)$, $k_{e,\theta}(a_\theta)$, $c_{e,h}(a_h)$ and $c_{e,\theta}(a_\theta)$. In previous studies, these quantities have been obtained either experimentally, through centrifuge testing [11], or analytically, by employing the Preisach hysteresis formalism [12]. In the present work, they are evaluated numerically using the Discrete Element Method (DEM) to explicitly account for the inherent variability of soil arising from particle-scale heterogeneity.

DEM simulations, inspired by centrifuge modelling principles, are performed using the open-source code YADE [19]. A three-step procedure is adopted: (1) calibration of contact law parameters, (2) generation of the DEM model, and (3) execution of simulations followed by post-processing. In the DEM framework, the granular medium is modelled as an assembly of discrete particles interacting at contact points via spring–dashpot mechanisms. A major advantage of this approach is its ability to capture microstructural features of the material, including heterogeneity and dilative behaviour, which are often neglected in continuum-based formulations. The motion of each particle is tracked by numerically integrating its equations of motion at each time step, enabling a detailed and realistic simulation of soil response under dynamic loading conditions.

3 Results

The development of the numerical model was guided by the centrifuge tests carried out by Tsang et al. [20], which examined the performance of geosynthetic-reinforced rubber–soil mixtures (RSM) incorporating varying rubber contents. In those experiments, pure gravel was employed as the baseline for comparison. Based on their experimental setup, including geometry, material properties, and boundary conditions, a centrifuge-scaled numerical model was constructed to replicate the behaviour of a rectangular shallow foundation with plan dimensions of 18 m × 12 m. The foundation was analysed under two distinct soil conditions: (i) a homogeneous gravel layer and (ii) a composite profile consisting of an RSM layer underlain by gravel.

The *pure gravel* layer was modelled as a three-dimensional assembly of spherical particles, whose radii were randomly sampled from a granulometric distribution represented by a cumulative distribution function (CDF). Particle diameters ranged between 6.35 mm and 9.53 mm, with a median value $D_{50,G}$ = 7.3 mm. To simulate the *Rubber- Soil Mixture,* the gravel-based particle assembly was modified by substituting 30% of its total mass with rubber particles. The rubber inclusions were also modelled as discrete spheres with a median particle diameter of $D_{50,RSM}$ = 3.1 mm.

The footing was assumed to be rigid and shallowly embedded at a depth of 1 m. The surrounding soil domain extended 35.5 m in length, 26 m in width, and 7.5 m in depth. In configurations including the RSM, the additional layer covered an area of 22 m × 16 m with a thickness of 3 m. Figure 2 illustrates the corresponding reduced-scale model developed according to centrifuge scaling principles.

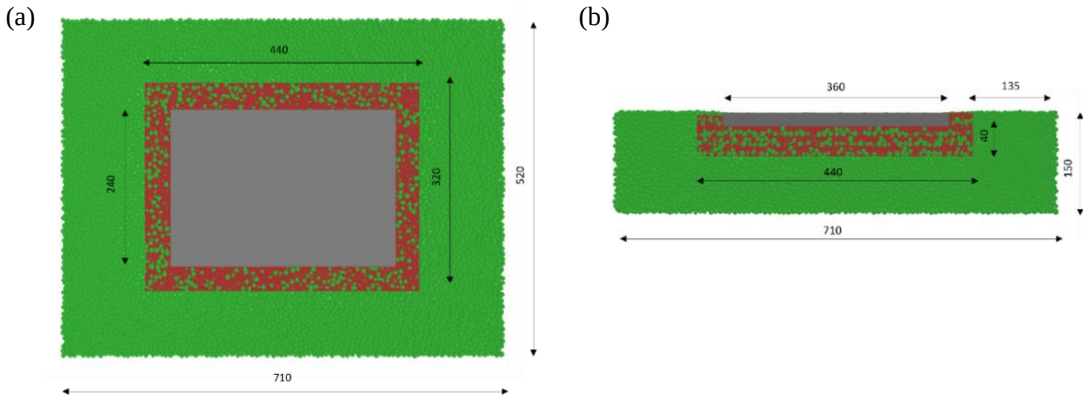

Figure 2: Reduced-scale model (dimensions in mm): (a) Top view; (a) Lateral view.

The optimal contact and mechanical model parameters, summarised in Table 1, were identified by calibrating the numerical simulations to match the experimentally observed shear modulus degradation and damping ratio curves, as functions of shear strain amplitude, reported in [21] and [22].

Parameter	*Gravel*	*Rubber*
Density, ρ [kg/m³]	2650	1200
Poisson's ratio, v	0.12	0.48
Young modulus E, *Pa*	1×10^{9}	$1\times10^{9}/350$
Inter-particle friction coefficient, μ	0.7 (35)	0.83 (40)
Number of particles (1 pack)	265000	470000
Timestep [s]	2.11×10^{-6}	1.57×10^{-6}

Table 1: Model Parameters.

A total of 300 independent particle assemblies were generated for each SSI configuration (i.e., gravel-only and RSM). All simulations were conducted under an enhanced gravitational field of 50g to replicate prototype stress conditions. The

simulations were performed on a high-performance computing (HPC) cluster, with the generation of each assembly parallelised across multiple compute nodes to ensure computational efficiency. Within each assembly, particle placement followed a Monte Carlo procedure governed by four independent random variables: the three spatial coordinates, sampled from uniform distributions, and the particle radius, drawn from the prescribed particle size distribution. Representative samples from the generated assemblies are shown in Figure 3.

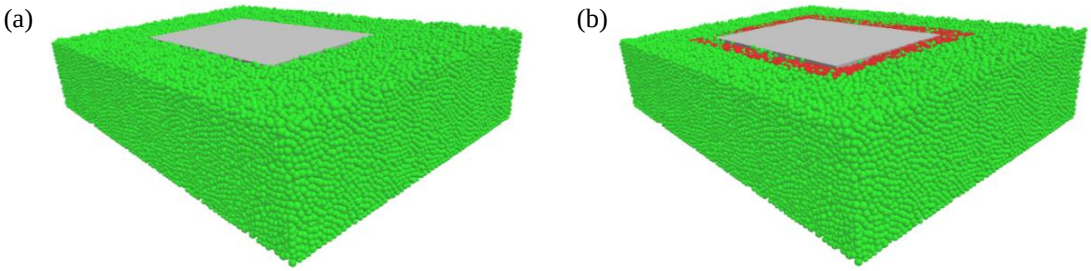

Figure 3: Samples of randomly generated SSI models: (a) Gravel-only; (b) RSM.

Stiffness translational and rotational curves from each simulation are presented as functions of the amplitudes a_h and a_θ in Figure 4. Specifically, the first row of the figure refers to the translational stiffness, whereas the second one to the rotational stiffness. Additionally, the subfigures on the left are related to the gravel-only configurations, while those on the right to configurations including the RSM layer. Each black curve represents the individual simulation outcome.

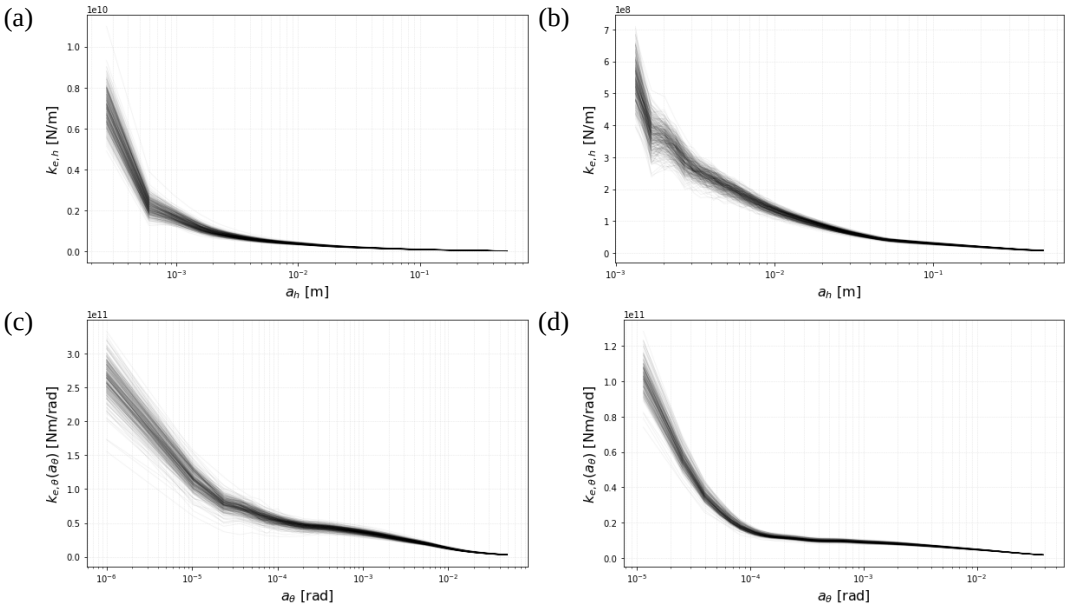

Figure 4: Translational stiffness of the shallow foundation: (a) Gravel-only; (b) RSM. Rotational stiffness of the shallow foundation: (c) Gravel-only; (d) RSM.

The results indicate that both the mean values and the associated variability of the system response decrease significantly with increasing displacement amplitude,

exhibiting a trend toward asymptotic stabilisation. This behaviour suggests a diminishing influence of initial uncertainties in the SSI models at larger deformation levels. When comparing the gravel-only and RSM configurations, the gravel-only case displays higher mean stiffness values, as anticipated, along with slightly greater variability across the ensemble.

Figure 5 shows the damping translational (Figures 5a and 5b) and rotational (Figures 5c and 5d) curves. Also in this case, Figures 5a and 5c, on the left, refer to the grave-only configurations, whereas, Figures 5b and 5d, on the right, pertain to configurations with RSM.

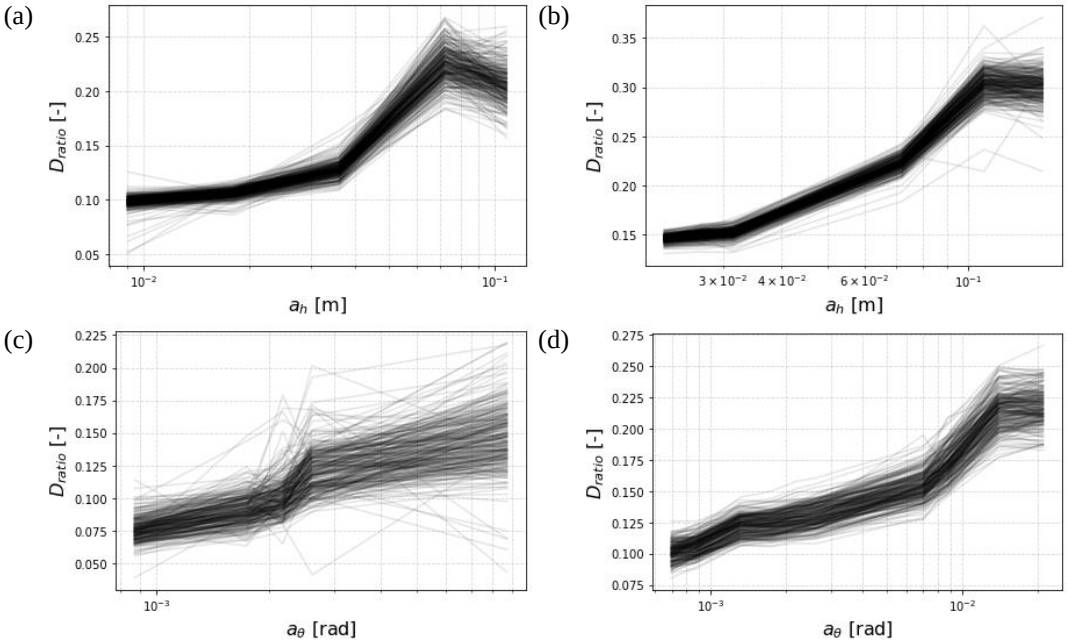

Figure 5: Translational damping of the shallow foundation: (a) Gravel-only; (b) RSM. Rotational damping of the shallow foundation: (c) Gravel-only; (d) RSM.

In contrast to the trend observed for stiffness, the variability in damping values increases with displacement amplitude. This behaviour is likely attributed to the growing uncertainty associated with the progressive widening of hysteresis loops at higher deformation levels. A comparison between the two configurations reveals that the RSM case exhibits higher mean damping values, while also demonstrating reduced variability relative to the gravel-only configuration.

The superstructure geometrical and mechanical parameters necessary for the model are reported in Table 2 [22]. Using these data, the steady state response is then determined for each realization of soil pack.

Data	*Value*
H [m] height of the superstructure	10
m [Mg] mass of the superstructure	650
m_F [Mg] mass of the foundation	260
I_F [Mg m^2] moment of inertia of the foundation	5.62x10^3
T [s] fundamental period of the superstructure assumed fully fixed	0.37
ζ damping ratio of the superstructure	0.05

Table 2: Mechanical and Geometrical Parameters of the 3-DoF structural model.

Figure 6 presents the variability of the top displacement for three selected values of the input amplitude p_0. From top to bottom, the three rows of Figure 6 refer to amplitudes p_0 = 5000N, p_0 = 10000N, and p_0 = 20000N, respectively. The left column (Figures 6a-c) refers to gravel-only configurations, while the right column (Figures 6d-f) refers to configurations with RSM. For both soil types, the results clearly indicate a nonlinear softening response as the load amplitude increases. The case with RSM shows a slightly larger dispersion of the results.

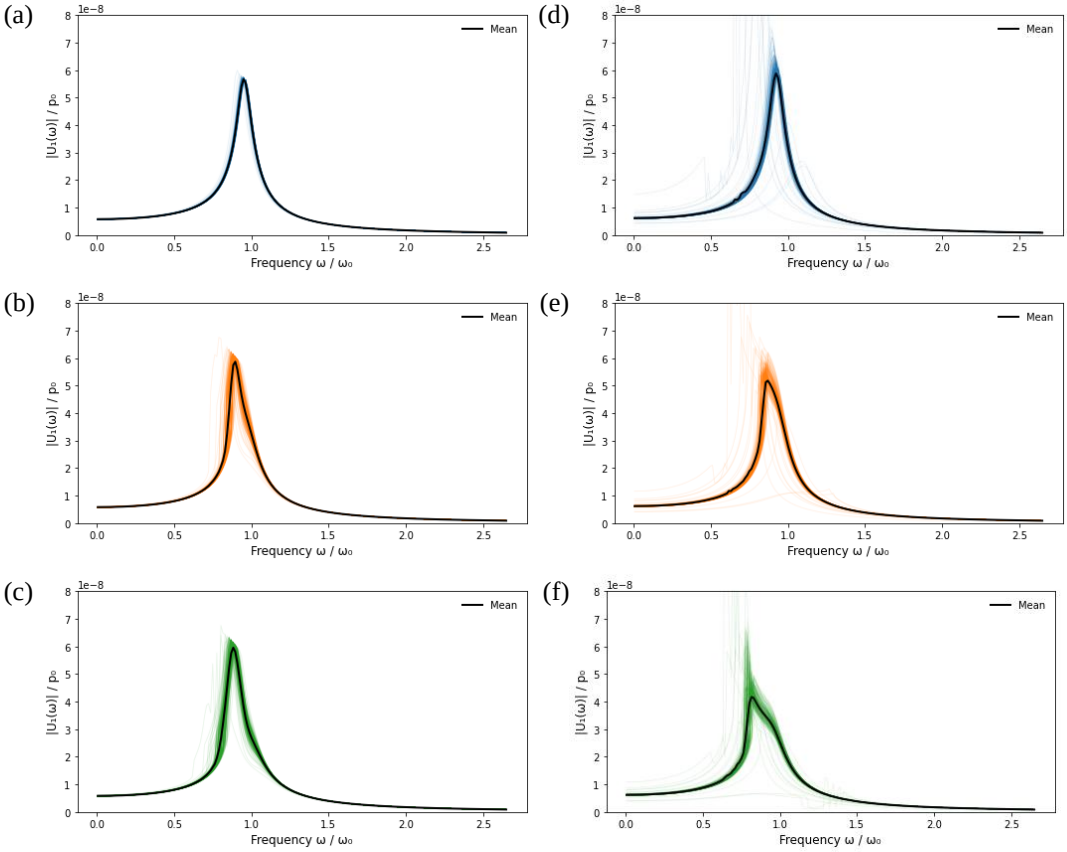

Figure 6: Steady state response variability: (a-c) Gravel-only with (a) p_0 = 5000N, (b) p_0 = 20000N, and (c) p_0 = 30000N; (d-f) RSM with (d) p_0 = 5000N, (e) p_0 = 20000N, and (f) p_0 = 30000N.

Finally, the variability of the equivalent period $T_e(a_h, a_\theta)$

$$\frac{T_e(a_h,a_\theta)}{T} = \sqrt{1 + \frac{k}{k_{e,h}(a_h)} + \frac{k\,H^2}{k_{e,\theta}(a_\theta)}} \tag{18}$$

of the nonlinear SSI system under the hypothesis of massless rigid foundation [12] is explored.

The results in Figure 7 clarify that the equivalent period is affected by both the rotational amplitude a_θ and the translational amplitude a_h in the range of explored values. Moreover, the increment of the fundamental period due to the SSI is, as expected larger when considering the GSI-RSM layer. Variability due to the soil pack soil particle distribution is also evident for both soil conditions.

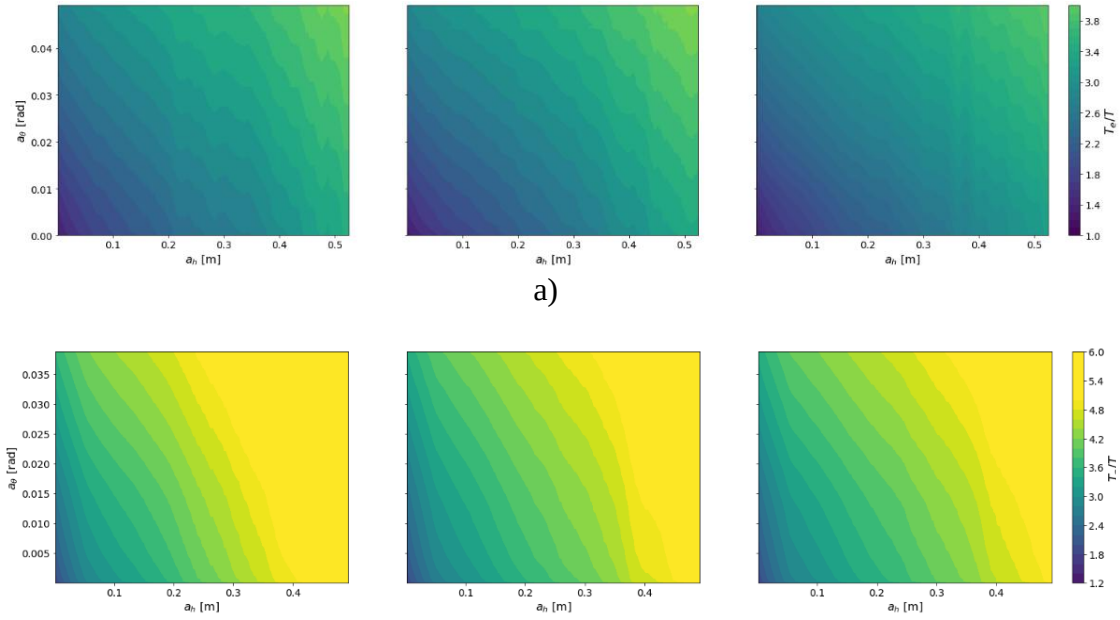

Figure 7: Contour maps of the equivalent SSI period variability for three randomly selected simulations a) Gravel-only; b) RSM.

4 Conclusions and Contributions

In this study, a comprehensive numerical framework was developed to investigate the steady-state harmonic response of nonlinear soil–structure interaction systems. The approach integrated a simplified 3-DoF lumped mass model with amplitude-dependent stiffness and damping properties derived using the harmonic balance method. To account for the inherent variability in soil behaviour, a Monte Carlo analysis was conducted based on discrete element method simulations of gravel and rubber–soil mixture foundations. These simulations captured the influence of particle-scale randomness on the equivalent dynamic properties of shallow foundations. The resulting statistical distributions of stiffness, damping, and equivalent fundamental period were analysed to assess the variability introduced by soil heterogeneity.

The findings indicate a clear nonlinear softening behaviour with increasing excitation amplitude, particularly in terms of stiffness reduction and period elongation. While the variability in stiffness tends to decrease at larger displacements, the damping variability increases, especially due to the widening of hysteresis loops. Comparisons between gravel-only and RSM configurations showed that the inclusion of rubber particles led to higher damping values and reduced variability, suggesting improved energy dissipation and robustness. Overall, the methodology provides a robust tool for quantifying soil–structure interaction effects under uncertain soil conditions and supports the development of performance-based design strategies for foundations subjected to dynamic loading.

References

[1] E. Kausel, "Early history of soil–structure interaction", Soil Dynamics and Earthquake Engineering, 30(9), 822–832, 2010.

[2] H.G. Poulos, E.H. Davis, "Elastic solutions for soil and rock mechanics", New York: Wiley, 1973.

[3] R. Dobry and G. Gazetas, "Dynamic Response of Arbitrarily Shaped Foundations", Journal of Geotechnical Engineering, 112(2), 109–135, 1986.

[4] C. Bolisetti, A.S. Whittaker, J.L. Coleman, "Linear and nonlinear soil-structure interaction analysis of buildings and safety-related nuclear structures," Soil Dynamics and Earthquake Engineering, 107, 218–233, 2018.

[5] M. Ciampoli and P.E. Pinto, "Effects of Soil-Structure Interaction on Inelastic Seismic Response of Bridge Piers", Journal of Structural Engineering, 121(5), 806–814, 1995.

[6] R. Dobry, "Simplified methods in Soil Dynamics", Soil Dynamics and Earthquake Engineering, 61–62, 246–268, 2014.

[7] G. Gazetas, I. Anastasopoulos, O. Adamidis, Th. Kontoroupi, "Nonlinear rocking stiffness of foundations", Soil Dynamics and Earthquake Engineering, 47, 83–91, 2013.

[8] I. Anastasopoulos, Th. Kontoroupi, "Simplified approximate method for analysis of rocking systems accounting for soil inelasticity and foundation uplifting", Soil Dynamics and Earthquake Engineering, 56, 28–43, 2014.

[9] I. Anastasopoulos, L. Sakellariadis, A. Agalianos, "Seismic analysis of motorway bridges accounting for key structural components and nonlinear soil–structure interaction", Soil Dynamics and Earthquake Engineering, 78, 127–141, 2015.

[10] Y. Lu, A.M. Marshall, I. Hajirasouliha, "A simplified Nonlinear Sway-Rocking model for evaluation of seismic response of structures on shallow foundations", Soil Dynamics and Earthquake Engineering, 81, 14–26, 2016.

[11] Z. Li, S. Escoffier, and P. Kotronis, "Study on the stiffness degradation and damping of pile foundations under dynamic loadings", Engineering Structures, 203, 109850, 2020.

[12] P. Cacciola, A. Tombari, "Steady state harmonic response of nonlinear soil-structure interaction problems through the Preisach formalism", Soil Dynamics and Earthquake Engineering, 44, 106669, 2021.

[13] P. Cacciola, I. Caliò, N. Fiorini, G. Occhipinti, D. Spina, A. Tombari, "Seismic response of nonlinear soil-structure interaction systems through the Preisach formalism: the Messina Bell Tower case study", Bulletin of Earthquake Engineering, 20, 3485–3514, 2021.
[14] A.H. Valdés, E. Torres, G. Camata, M. Petracca, J.F.G. Crempien, J.A. Abell, "Impact of Soil–Structure Interaction Modeling Simplifications and Structural Nonlinearity on Uncertainty in EDPs: A Case Study on an Existing RC Building in Santiago", Earthquake Engineering & Structural Dynamics, 2025.
[15] F.S. Wong, "Uncertainties in Dynamic Soil Structure Interaction", Journal of Engineering Mechanics, 110, 308–32, 1984.
[16] W.D. Iwan, "A Distributed-Element Model for Hysteresis and Its Steady-State Dynamic Response", Journal of Applied Mechanics, 33(4), 893–900, 1966.
[17] P.D. Spanos, "Hysteretic structural vibrations under random load", The Journal of the Acoustical Society of America, 65(2), 404–410, 1979.
[18] P.D. Spanos, A. Kontsos, P. Cacciola, "Steady-State Dynamic Response of Preisach Hysteretic Systems", Journal of Vibration and Acoustics, 128(2), 244–250, 2006.
[19] V. Šmilauer, V. Angelidakis, E. Catalano, R. Caulk, B. Chareyre, W. Chèvremont, S. Dorofeenko, J. Duriez, N. Dyck, J. Eliáš, B. Er, A. Eulitz, A. Gladky, N. Guo, C. Jakob, F. Kneib, J. Kozicki, D. Marzougui, R. Maurin, C. Modenese, G. Pekmezi, L. Scholtès, L. Sibille, J. Stransky, T. Sweijen, K. Thoeni, C. Yuan, "Yade Documentation (3rd ed.)", The Yade Project, 2021, doi:10.5281/zenodo.5705394
[20] H.H. Tsang, D.P. Tran, W.Y., Hung, K., Pitilakis, K., E.F. Gad, "Performance of geotechnical seismic isolation system using rubber–soil mixtures in centrifuge testing". Earthquake Engineering & Structural Dynamics, 50(5), 1271-1289, 2021.
[21] K. Senetakis, A. Anastasiadis, K. Pitilakis, "Dynamic properties of dry sand/rubber (RSM) and gravel/rubber (GRM) mixtures in a wide range of shearing strain amplitudes", Soil Dynamics and Earthquake Engineering, 33, 38-53, 2012.
[22] H.H. Tsang, K. Pitilakis, "Mechanism of geotechnical seismic isolation system: Analytical modelling", Soil Dynamics and Earthquake Engineering, 122, 171-184, 2019.